

Article

Deep Learning-Based Radiomics for Prognostic Stratification of Low-Grade Gliomas Using a Multiple-Gene Signature

Mert Karabacak ^{1,†} , Burak B. Ozkara ^{2,†} , Kaan Senparlak ^{3,†} and Sotirios Bisdas ^{2,4,*} 

¹ Department of Neurosurgery, Mount Sinai Health System, 1468 Madison Avenue, New York, NY 10029, USA; mert.karabacak@mountsinai.org

² Department of Neuroradiology, MD Anderson Cancer Center, 1400 Pressler Street, Houston, TX 77030, USA; bbozkara@mdanderson.org

³ School of Computation, Information, and Technology, Technical University of Munich, Theresienstr. 90, Bayern, 80333 Munich, Germany; kaansenparlak@hotmail.com

⁴ Department of Neuroradiology, The National Hospital for Neurology and Neurosurgery, University College London NHS Foundation Trust, London WC1N 3BG, UK

* Correspondence: s.bisdas@ucl.ac.uk; Tel.: +44-020-3448-3446

† These authors contributed equally to this work.

Abstract: Low-grade gliomas are a heterogeneous group of infiltrative neoplasms. Radiomics allows the characterization of phenotypes with high-throughput extraction of quantitative imaging features from radiologic images. Deep learning models, such as convolutional neural networks (CNNs), offer well-performing models and a simplified pipeline by automatic feature learning. In our study, MRI data were retrospectively obtained from The Cancer Imaging Archive (TCIA), which contains MR images for a subset of the LGG patients in The Cancer Genome Atlas (TCGA). Corresponding molecular genetics and clinical information were obtained from TCGA. Three genes included in the genetic signatures were WEE1, CRTAC1, and SEMA4G. A CNN-based deep learning model was used to classify patients into low and high-risk groups, with the median gene signature risk score as the cut-off value. The data were randomly split into training and test sets, with 61 patients in the training set and 20 in the test set. In the test set, models using T1 and T2 weighted images had an area under the receiver operating characteristic curve of 73% and 79%, respectively. In conclusion, we developed a CNN-based model to predict non-invasively the risk stratification provided by the prognostic gene signature in LGGs. Numerous previously discovered gene signatures and novel genetic identifiers that will be developed in the future may be utilized with this method.

Keywords: deep learning; radiomics; neural networks; gliomas; LGG; gene signatures



Citation: Karabacak, M.; Ozkara, B.B.; Senparlak, K.; Bisdas, S. Deep Learning-Based Radiomics for Prognostic Stratification of Low-Grade Gliomas Using a Multiple-Gene Signature. *Appl. Sci.* **2023**, *13*, 3873. <https://doi.org/10.3390/app13063873>

Academic Editor: Jan Egger

Received: 17 February 2023

Revised: 15 March 2023

Accepted: 17 March 2023

Published: 18 March 2023



Copyright: © 2023 by the authors. Licensee MDPI, Basel, Switzerland. This article is an open access article distributed under the terms and conditions of the Creative Commons Attribution (CC BY) license (<https://creativecommons.org/licenses/by/4.0/>).

1. Introduction

Precision oncology calls for finer characterization of tumors than the current classifications, enabling more patient-specific treatment and, thus, better outcomes. Low-grade gliomas (LGGs) form a heterogeneous group of infiltrative neoplasms with astrocytic and oligodendroglial morphology [1]. They differ significantly in progression-free survival (PFS) and overall survival (OS) [2]. Some LGGs rapidly progress to glioblastomas (GBM (WHO grade IV)), while others will progress slower or remain stable [3,4]. Moreover, their treatment response varies significantly, with survival ranging from 1 to 15 years [3,4]. These differences in prognosis and response to treatment are mainly due to the high molecular heterogeneity caused by different genetic alterations during tumor development [5,6]. Hence, genomic biomarkers were first integrated into the WHO Classification of Tumors of the Central Nervous System (CNS) in 2016 [5] to explain the variability in the LGGs' behavior, and the number of genomic identifiers has recently increased in the 2021 fifth edition classification [7]. IDH mutations [8], 1p/19q codeficiency [9], ATRX mutation [10], and TERT promoter mutation [11] are among the known prognostic molecular markers for

LGGs. However, the complex genetic mechanisms and heterogeneity of LGGs require more prognostic markers to explore better risk stratification strategies and efficient treatment modalities. Genetic signatures integrating multiple biomarkers are believed to be superior to single predictive biomarkers [12]. In recent years, gene signatures integrating multiple genes were proposed for LGGs. Zeng et al. reported a 3-gene (EMP3, GSX2, EMILIN3) prognostic signature [13]; Zhang et al. reported a 4-gene (EMP3, GNG12, KIF2C, IFI44) model [14]; and Xiao et al. constructed a 3-gene (WEE1, CRTAC1, SEMA4G) signature [12]. In the study by Xiao et al., the proposed model was proved to have better prognostic value in predicting 1-, 3- and 5-year OS rates than other models [12].

Within the limits of the current technology, genetic and molecular profiling of gliomas has a few drawbacks. First, it requires direct tumor sampling, which involves invasive procedures such as surgical resection or biopsy. Since the standard of care for LGGs include surgical removal of the tumor in many cases, it is not too much to say that the samples obtained during the surgery will not allow tailored surgical strategies [1]. Multiple biopsy-based approaches may allow more patient-specific treatment, but the diagnostic information that biopsy yields may be limited due to sampling error and intratumor heterogeneity [15,16]. On the other hand, high cost and time-consuming remain serious shortcomings for the widespread clinical use of conventional genetic and molecular profiling methods [17,18]. For these reasons, noninvasive determination of genetic and molecular profiles could allow more individualized treatment options and prognostication for the patients.

Radiomics is a generic term to refer to the analytical technologies in medical imaging and the image features obtained by this approach. Research on the relationship between medical images and the genome is called ‘radiogenomics’. Radiomics allow the characterization of imaging phenotypes with high-throughput extraction of quantitative imaging features from radiologic images [19]. Commonly, the radiomic approach includes image acquisition, preprocessing of the images, region of interest (ROI) delineation (segmentation), feature extraction, selection of the most relevant features, and building predictive models for the desired outcome [20]. Extracted radiomic features in many studies are pre-engineered or handcrafted, such as shape, intensity, texture, and wavelet features. These are usually low-order features, even if their number can reach thousands. Most of the studies in the literature utilized different machine learning algorithms using these extracted and selected radiomic features for model construction [21]. Deep learning offers better-performing models and a simplified pipeline by automatic feature learning. Convolutional neural networks (CNNs) are one form of deep learning that consists of a series of chained convolutional layers followed by an output vector of class probabilities [22]. Multiple convolutional layers with non-linear activation functions allow the learning of complex features. CNNs have shown promising capabilities in automatic segmentation [23,24], classification of molecular subtypes in gliomas [25,26], and survival outcomes [27,28].

To our knowledge, no previous study has applied a deep learning-based radiomic approach for novel biomarkers, such as the aforementioned multiple-gene genetic signatures. Our study utilized the 3-gene signature that stratifies LGG patients into high- and low-risk groups, according to Xiao et al. [14]. We aimed to determine whether neuroimaging features on preoperative MRI studies entered into a CNN pipeline could facilitate the proposed LGG stratification.

2. Materials and Methods

2.1. Patient Cohort

The results shown here are in whole or part based upon data generated by The Cancer Genome Atlas (TCGA) Research Network (<http://cancergenome.nih.gov/>) and The Cancer Imaging Archive (TCIA) (accessed on 18 May 2022) [29,30]. No institutional review board approval was required to use information from TCIA and TCGA databases in the present study since these databases contain publicly available datasets in which all data are anonymized. MRI data were retrospectively obtained from TCIA, which contains MR

images for a subset of the LGG patients from TCGA. Corresponding molecular genetics and clinical information were obtained from TCGA. There were no missing data.

We used a candidate prognostic three-gene signature biomarker developed in a recent publication for LGG as the genomic classifier [12]. Genomic data came from TCGA-LGG collection and were based on RNA-seq data. Based on the proposed gene signature model, the risk score $[(0.4470 \times \text{expression level of WEE1}) + (-0.1530 \times \text{expression level of CRTAC1}) + (-0.3723 \times \text{expression level of SEMA4G})]$ of each patient was calculated. Patients were divided into low- and high-risk groups, with the median risk score as the cut-off value. In the original publication, the high-risk group had significantly poorer survival results than the low-risk group (hazard ratio (low-risk vs. high-risk) = 0.198, 95% CI (0.120–0.325)) with this classification [12].

All patients identified met the following criteria: (i) pathologically confirmed WHO grade II and III gliomas; (ii) available preoperative MR imaging consisting of pre-contrast axial T1-weighted (T1), post-contrast axial T1-weighted (T1C), axial T2-weighted (T2), and T2-weighted fluid attenuation inversion recovery (FLAIR) images; (iii) available genomic data for calculation of the adopted gene signature; (iv) available clinical data including age, sex, and Karnofsky performance status (KPS); (v) available ROI segmentations supplied in TCIA.

2.2. Image Preprocessing and Segmentation

All MR images were downloaded via the National Biomedical Imaging Archive (NBIA) Data Retriever (version 4.3, The Cancer Imaging Archive, Bethesda, MD, USA, <https://wiki.cancerimagingarchive.net/display/NBIA/Downloading+Images+Using+the+NBIA+Data+Retriever>, accessed on 20 March 2021) and were converted from DICOM to NifTI format using dcm2niix (version 1.0, Chris Rorden, <https://github.com/rordenlab/dcm2niix>, accessed on 20 March 2021) [31]. To remove intensity nonuniformity with low-frequency, N4 bias field correction was applied [32]. Skull stripping was then applied using the Brain Extraction Tool (BET) from the Functional Magnetic Resonance Imaging of the Brain (FMRIB) software library (version 1.1, FMRIBGroup, Oxford, United Kingdom; <http://www.fmrib.ox.ac.uk/fsl/>, accessed on 21 March 2021) [33]. All imaging modalities (T1C, T1, T2, FLAIR) were co-registered using the FMRIB's Linear Image Registration Tool (FLIRT; <http://www.fmrib.ox.ac.uk/fsl/fslwiki/FLIRT>, accessed on 20 March 2021) [34]. Registration with a linear affine transformation algorithm using 12 degrees of freedom, trilinear interpolation, and a mutual-information cost function was implemented. The reference volume was the postcontrast axial T1-weighted acquisition. After image registration, signal intensity normalization was performed using the WhiteStripe R package [35]. We obtained region-of-interest (ROI) masks drawn for the four MRI sequences (T1C, T1, T2, and FLAIR) for 81 patients from the previous study by Zhou et al. [36].

2.3. Convolutional Neural Network and Model Implementation

We designed our neural network to consist of 7 main sections, including the input and the output layers. Three of these main sections employ 3D convolutional layers, which have different numbers of filters and kernel sizes. These hyperparameters are fine-tuned with controlled experiments to reach the model with the best pattern recognition capabilities for our input data. After every 3D convolutional layer, a max pooling layer was employed, reducing the dimensionality of its input to allow for sharper patterns to be recognized. The dimensionality reduction also decreased the network complexity. Finally, batch normalization was integrated at the end of these three main sections. Batch normalization allowed for using much higher learning rates and being less careful about initialization while also acting as a regularizer [37]. A global average pool layer provided the transition from 3D to 1D by averaging the neuron values in 2 dimensions. Global average pooling enforced correspondence between feature maps and categories and acted as a structural regularizer [38]. Fully connected layers were used with dropout layers to

prevent overfitting before completing the network with a sigmoid-activated output layer. The network structure is shown in Figure 1.

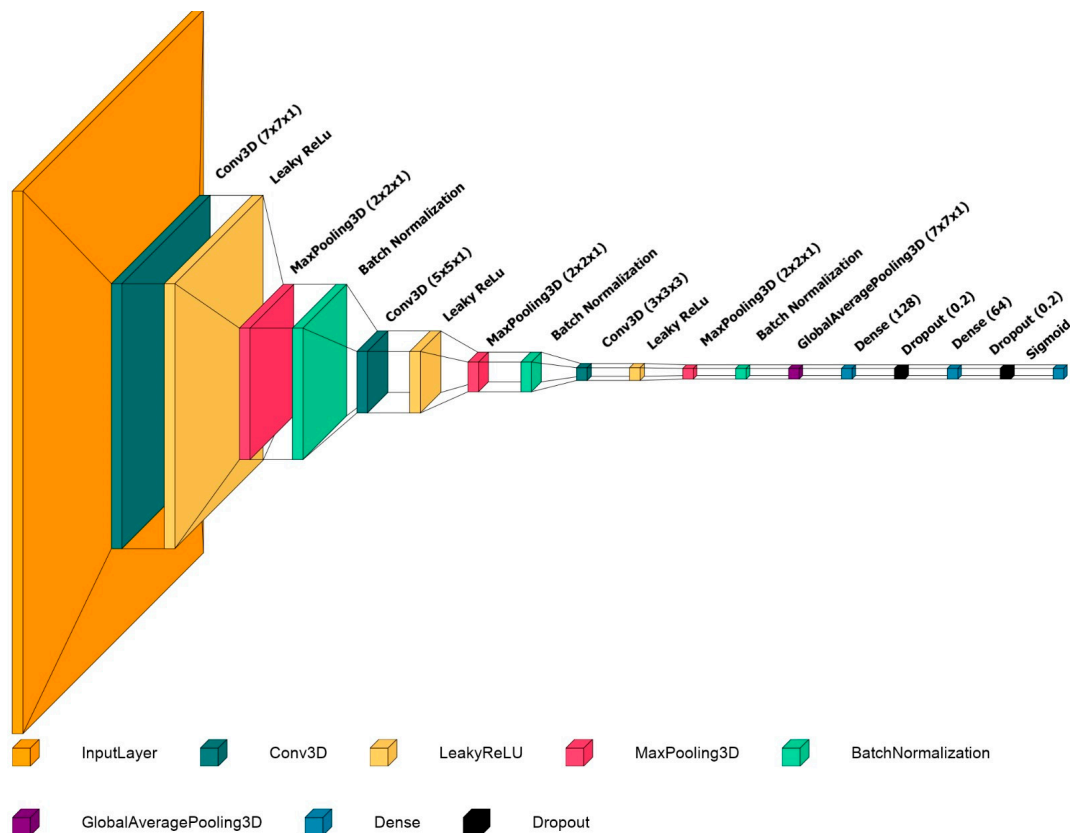


Figure 1. The network structure.

Keras API was used with the PlaidML for AMD graphical processing unit (GPU) package as the backend in our implementation. Non-linear activation functions were utilized in every layer, including Leaky ReLU for 3D Convolutional layers and ReLU for fully connected layers. A widely adopted sigmoid classifier with a binary cross-entropy objective function was used to classify inputs in the final layer as low-risk or high-risk. The weight optimization was done with Adamax, a generalized version of the Adam optimizer. The Adam optimizer is easy to implement, computationally efficient, has minor memory requirements, is invariant to diagonal rescaling of the gradients, and is well suited for significant problems in terms of data and parameters [39]. A batch size of 2 was used, leading to longer training times and higher model quality. We trained the network on an AMD Radeon Pro 5300M GPU.

2.4. Model Evaluation

The data were randomly split into training and test sets, with 61 patients in the training set and 20 patients in the test set. To compensate for the data scarcity, a data augmentation method was employed. While training the network, new training data was generated using random rotations up to 90 degrees on existing data. This method prevented the model from overfitting to the train set. The primary evaluation metric of the binary classifier was the test set classification accuracy. The area under the curve (AUC) of the receiver operating characteristic (ROC) and F1-score were additional metrics considered when evaluating the model.

2.5. Statistical Analysis

All statistical analyses were performed in R 4.1.3 [40] with RStudio 2022.02.1+461 [41]. The normality of data distributions was assessed via the Shapiro-Wilk test. The descriptive analyses were reported as means \pm standard deviations for normally distributed variables, medians (interquartile ranges) for non-normally distributed variables, and frequencies for categorical variables. Group differences were tested using the independent *t*-test for normally distributed variables with equal variances, the Mann-Whitney U test for non-normally distributed variables, or the chi-square test for categorical variables. A two-tailed *p*-value of 0.05 was considered to indicate statistical significance.

2.6. Source Code

The source code for the described methods is available on GitHub (mertkarabacak/LGG-GS (<https://github.com/mertkarabacak/LGG-GS>, accessed on 20 March 2021)).

3. Results

3.1. Patient Characteristics

The average age was 45.8 years. Thirty-eight subjects were female, and 43 were male. Among 81 patients, 24 were astrocytomas, 24 were oligoastrocytomas, and 33 were oligodendrogliomas. Regarding tumor grade, 33 were of grade II, and 48 were of grade III. No statistical difference was found for any variables, including the gene expression values, between training and test sets. The patient characteristics are described in Table 1.

Table 1. Patient characteristics.

Variables	Training Set (n = 61)	Test Set (n = 20)	<i>p</i> Value	High Risk (n = 54)	Low Risk (n = 27)	<i>p</i> Value
Age at diagnosis	45.2 (14.4)	47.6 (11.6)	0.454	44.6 (13.1)	48.2 (14.8)	0.291
Gender						
Male	31 (50.8%)	12 (60%)	0.649	29 (53.7%)	14 (51.9%)	1.000
Female	30 (49.2%)	8 (40%)		25 (47.3%)	13 (48.1%)	
Histologic Diagnosis						
Astrocytoma	18 (29.5%)	6 (30%)	0.789	8 (14.8%)	16 (59.3%)	0.000
Oligoastrocytoma	17 (27.9%)	7 (35%)		17 (31.5%)	7 (25.9%)	
Oligodendroglioma	26 (42.6%)	7 (35%)		29 (53.8%)	4 (14.8%)	
Grade						
II	24 (39.3%)	9 (45%)	0.854	29 (53.7%)	4 (14.8%)	0.002
III	37 (60.7%)	11 (55%)		25 (47.3%)	23 (85.2%)	
Risk Status						
High	41 (67.2%)	13 (65%)	1.000	-	-	
Low	20 (32.8%)	7 (35%)		-	-	
Gene expression						
WEE1	7.8 (1.3)	7.9 (1)	0.5254	7.3 (0.9)	9.0 (1)	0.000
CRTAC1	9.9 (9.3–10.7)	9.7 (8.7–10.4)	0.7425	10.3 (9.5–10.9)	8.4 (7.5–9.4)	0.000
SEMA4G	8.3 (8–8.7)	8.2 (8–8.5)	0.7633	8.5 (8.2–8.7)	7.8 (7.0–8.2)	0.000

3.2. Model Performance

Two models were trained with two separate input types. The first input type was T1-weighted (T1), and on the training set, the model had accuracy, sensitivity, specificity, precision, and AUC of 85%, 65%, 95%, 86%, and 94%, respectively. On the test set, the model with the T1 input type had accuracy, sensitivity, specificity, precision, and AUC of 80%, 57%, 92%, 80%, and 73%, respectively. For the input type T2-weighted (T2), the model had accuracy, sensitivity, specificity, precision, and AUC of 79%, 100%, 73%, 68%, and 94%, respectively, on the training set. On the test set, the model with the T2 input type had accuracy, sensitivity, specificity, precision, and AUC of 75%, 100%, 62%, 58%, and 79%, respectively. The model performances are described in Table 2. Figure 2 depicts the ROC

curve of the model using T1-WI as input, and Figure 3 depicts the ROC curve of the model using T2-WI as input.

Table 2. Model performances.

	Training Set					Test Set				
	Accuracy	AUC	Sensitivity	Specificity	Precision	Accuracy	AUC	Sensitivity	Specificity	Precision
T1	0.85	0.94	0.65	0.95	0.86	0.8	0.73	0.57	0.92	0.8
T2	0.79	0.94	1	0.73	0.68	0.75	0.79	1	0.62	0.58

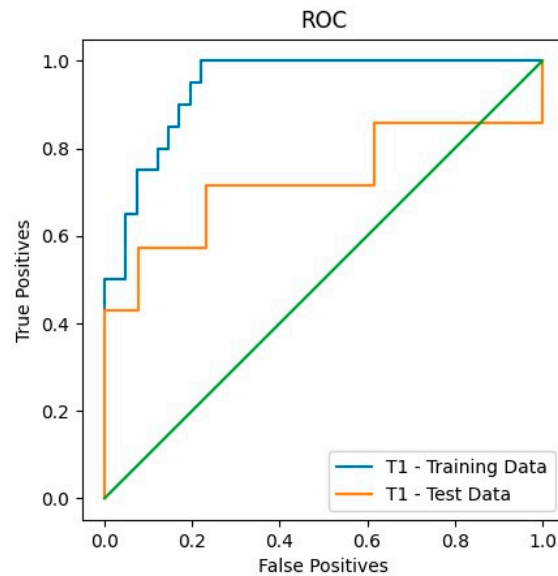


Figure 2. Receiver operating characteristic curve of the model using T1-weighted images as input.

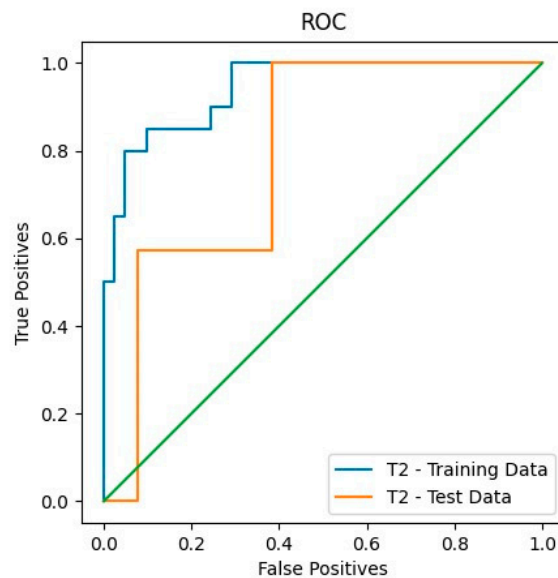


Figure 3. Receiver operating characteristic curve of the model using T2-weighted images as input.

4. Discussion

Significant advances have been made in the exploration of the molecular pathology of gliomas in recent years. Many molecular markers have been discovered that are useful for clinical diagnosis, prognostic evaluation, and treatment guidance, such as IDH1/2 gene mutation and chromosome 1p/19q co-deletion [8,9] but can only partially explain the

prognosis of gliomas at present. Therefore, further efforts are needed to improve prognostic accuracy and facilitate therapeutic approaches.

In addition to molecular markers, recent studies have identified gene expression profiles that make it possible to categorize patients into high- and low-risk groups regarding survival probabilities. Gene signatures have attracted much attention in recent years and have shown great potential for prognostic prediction in LGG patients. Zhang et al. constructed a five-gene signature that can predict the individual clinical outcome with high accuracy in LGG patients [42]. Liu et al. developed a ten-gene signature that successfully classified LGGs into groups with different prognostic probabilities [43]. Zhang et al. constructed a robust six-immune-related gene signature and established a prognostic nomogram for risk stratification and prediction of overall survival in LGG patients [44]. The risk score calculation, based on the three-gene signature we adopted in our study, was a significant prognostic factor after adjusting for the effects of age, sex, tumor grade, and treatment modalities. Xiao et al. identified a three-gene model that showed satisfactory performance in predicting 1-, 3-, and 5-year survival of LGG patients [12]. The AUC value of classification into low- and high-risk groups in 1-, 3- and 5-year survival graphs was greater than 0.75, regardless of the training or validation set.

In the current clinical context, determining molecular markers or gene signatures of gliomas requires invasive procedures, such as surgical resection or biopsy. Given the considerable high intra-tumor heterogeneity of the lesions and the risk that a tissue sampling may not adequately represent the overall genomic profile, imaging, which is performed at the very beginning of the diagnostic process of glioma cases, may be useful in assessing heterogeneity since the imaging data provides a complete view of the tumor. Hence, noninvasive characterization of genomic profiles would better aid clinicians in making more precise treatment and follow-up plans before surgery or biopsy. Genomic analyses could easily be replaced by models predicting the genetic and molecular profiles of the tumors based on imaging if they are highly accurate. Even models with moderate accuracy could potentially be incorporated into diagnostic and therapeutic paradigms.

In this study, we demonstrated the value of CNNs employed to post-process the radiomics information from conventional routine MRI from a publicly available multi-institutional dataset to predict a specific gene signature-based risk stratification status in LGG patients. To our knowledge, this is the first study that attempted to predict a gene signature-based risk stratification using imaging studies. The deep-learning model was developed and cross-validated for its performance. AUC values for the test sets were 0.80 and 0.75 for the T1 and T2 input models, respectively. We did not include any clinical parameters in our models, such as age or KPS. Because these alone have a significant impact on classifying the survival risk status of the patients, clinicians are already aware that high age or low KPS indicate likely poor survival outcomes. This method becomes very clinically useful when clinical parameters fail to inform providers in their decision-making process. We did not include WHO grade IV gliomas in our analysis either, since they have clinically distinct survival outcomes compared to LGGs. Identifying high-risk LGG patients early in the course of their disease may be important in clinical decision-making as it may guide clinicians through more aggressive treatment options and closer follow-ups.

Despite the promising results, there are a few limitations to be aware of. First, our sample size was relatively small (80 patients), especially considering that neural networks necessitate a massive amount of input for high-performing models. To address this limitation, we used data augmentation and tailored an optimized CNN structure. Second, we applied our proposed model to LGGs only. In clinical scenarios, it would be of higher value if GBMs were also included. Our methodology requires prior knowledge of the tumor grade. Though GBMs have distinct features, some LGG-appearing tumors are actually GBMs. To differentiate LGGs from GBMs at the baseline, advanced MRI techniques, such as diffusion MRI, perfusion MRI or MR spectroscopy, can be used. Furthermore, models predicting survival outcomes may show over-optimistic results if they are implemented in a dataset including both GBMs and LGGs since they have different survival rates inherently.

Third, our study includes only the T1- and T2-weighted MRI sequences. We did not utilize advanced MRI techniques, even though they have been shown to provide additional information and can improve prediction performance [45,46]. Yet, including these sequences is also a potential limitation because these sequences are unfortunately not widely available, just as we did not have them available for our dataset. Lastly, due to the small sample size and the lack of an external dataset containing both the genomic information we used in our study and imaging data, there was no independent test set in our study. Instead, we utilized a commonly used cross-validation technique.

5. Conclusions

In conclusion, we developed a CNN-based model to non-invasively predict a risk stratification offered by a prognostic gene signature in LGGs. This technique may be applied to many of the previously discovered gene signatures and novel genetic identifiers to be developed in the future. Importantly, our approach has the genuine potential to be incorporated into the clinical decision-making process.

Author Contributions: Conceptualization, M.K., B.B.O. and K.S.; methodology, M.K., B.B.O. and K.S.; software, M.K., B.B.O. and K.S.; validation, S.B.; formal analysis, M.K., B.B.O. and K.S.; investigation, M.K., B.B.O. and K.S.; resources, S.B.; data curation, M.K., B.B.O. and K.S.; writing—original draft preparation, M.K., B.B.O. and K.S.; writing—review and editing, M.K., B.B.O. and K.S.; visualization, M.K., B.B.O. and K.S.; supervision, S.B.; project administration, S.B. All authors have read and agreed to the published version of the manuscript.

Funding: This research received no external funding.

Institutional Review Board Statement: Ethical review and approval were waived for this study because only the information from public databases was used, which contain fully anonymized data.

Informed Consent Statement: Not applicable.

Data Availability Statement: The data presented in this study are openly available in The Cancer Genome Atlas Research Network and The Cancer Imaging Archive at <https://doi.org/10.7937/K9/TCIA.2016.L4LTD3TK>, and <https://doi.org/10.1007/s10278-013-9622-7> [29,30].

Conflicts of Interest: The authors declare no conflict of interest.

References

1. Brat, D.J.; Verhaak, R.G.W.; Aldape, K.D.; Yung, W.K.A.; Salama, S.R.; Cooper, L.A.D.; Rheinbay, E.; Miller, C.R.; Vitucci, M.; et al.; Cancer Genome Atlas Research Network. Comprehensive, Integrative Genomic Analysis of Diffuse Lower-Grade Gliomas. *N. Engl. J. Med.* **2015**, *372*, 2481–2498. [[CrossRef](#)]
2. Olar, A.; Sulman, E.P. Molecular Markers in Low-Grade Glioma—Toward Tumor Reclassification. *Semin. Radiat. Oncol.* **2015**, *25*, 155–163. [[CrossRef](#)]
3. Van den Bent, M.J. Interobserver Variation of the Histopathological Diagnosis in Clinical Trials on Glioma: A Clinician's Perspective. *Acta Neuropathol.* **2010**, *120*, 297–304. [[CrossRef](#)] [[PubMed](#)]
4. Van den Bent, M.J.; Brandes, A.A.; Taphoorn, M.J.B.; Kros, J.M.; Kouwenhoven, M.C.M.; Delattre, J.-Y.; Bernsen, H.J.J.A.; Frenay, M.; Tijssen, C.C.; Grisold, W.; et al. Adjuvant Procarbazine, Lomustine, and Vincristine Chemotherapy in Newly Diagnosed Anaplastic Oligodendroglioma: Long-Term Follow-up of EORTC Brain Tumor Group Study 26951. *J. Clin. Oncol.* **2013**, *31*, 344–350. [[CrossRef](#)] [[PubMed](#)]
5. Louis, D.N.; Perry, A.; Reifenberger, G.; Von Deimling, A.; Figarella-Branger, D.; Cavenee, W.K.; Ohgaki, H.; Wiestler, O.D.; Kleihues, P.; Ellison, D.W. The 2016 World Health Organization Classification of Tumors of the Central Nervous System: A summary. *Acta Neuropathol.* **2016**, *131*, 803–820. [[CrossRef](#)]
6. Appin, C.L.; Brat, D.J. Molecular Genetics of Gliomas. *Cancer J.* **2014**, *20*, 66–72. [[CrossRef](#)]
7. Louis, D.N.; Perry, A.; Wesseling, P.; Brat, D.J.; Cree, I.A.; Figarella-Branger, D.; Hawkins, C.; Ng, H.K.; Pfister, S.M.; Reifenberger, G.; et al. The 2021 WHO Classification of Tumors of the Central Nervous System: A summary. *Neuro. Oncol.* **2021**, *23*, 1231–1251. [[CrossRef](#)] [[PubMed](#)]
8. Batsios, G.; Viswanath, P.; Subramani, E.; Najac, C.; Gillespie, A.M.; Santos, R.D.; Molloy, A.R.; Pieper, R.O.; Ronen, S.M. PI3K/MTOR Inhibition of IDH1 Mutant Glioma Leads to Reduced 2HG Production That Is Associated with Increased Survival. *Sci. Rep.* **2019**, *9*, 10521. [[CrossRef](#)]
9. Zhang, G.-H.; Zhong, Q.-Y.; Gou, X.-X.; Fan, E.-X.; Shuai, Y.; Wu, M.-N.; Yue, G.-J. Seven Genes for the Prognostic Prediction in Patients with Glioma. *Clin. Transl. Oncol.* **2019**, *21*, 1327–1335. [[CrossRef](#)] [[PubMed](#)]

10. Ren, Y.; Zhang, X.; Rui, W.; Pang, H.; Qiu, T.; Wang, J.; Xie, Q.; Jin, T.; Zhang, H.; Chen, H.; et al. Noninvasive Prediction of IDH1 Mutation and ATRX Expression Loss in Low-Grade Gliomas Using Multiparametric MR Radiomic Features. *J. Magn. Reson. Imaging* **2019**, *49*, 808–817. [[CrossRef](#)]
11. Chan, A.K.-Y.; Yao, Y.; Zhang, Z.; Chung, N.Y.-F.; Liu, J.S.-M.; Li, K.K.-W.; Shi, Z.; Chan, D.T.-M.; Poon, W.S.; Zhou, L.; et al. TERT Promoter Mutations Contribute to Subset Prognostication of Lower-Grade Gliomas. *Mod. Pathol.* **2015**, *28*, 177–186. [[CrossRef](#)] [[PubMed](#)]
12. Xiao, K.; Liu, Q.; Peng, G.; Su, J.; Qin, C.-Y.; Wang, X.-Y. Identification and Validation of a Three-Gene Signature as a Candidate Prognostic Biomarker for Lower Grade Glioma. *PeerJ* **2020**, *8*, e8312. [[CrossRef](#)] [[PubMed](#)]
13. Zeng, W.-J.; Yang, Y.-L.; Liu, Z.-Z.; Wen, Z.-P.; Chen, Y.-H.; Hu, X.-L.; Cheng, Q.; Xiao, J.; Zhao, J.; Chen, X.-P. Integrative Analysis of DNA Methylation and Gene Expression Identify a Three-Gene Signature for Predicting Prognosis in Lower-Grade Gliomas. *Cell. Physiol. Biochem.* **2018**, *47*, 428–439. [[CrossRef](#)] [[PubMed](#)]
14. Zhang, C.; Yu, R.; Li, Z.; Song, H.; Zang, D.; Deng, M.; Fan, Y.; Liu, Y.; Zhang, Y.; Qu, X. Comprehensive Analysis of Genes Based on Chr1p/19q Co-Deletion Reveals a Robust 4-Gene Prognostic Signature for Lower Grade Glioma. *Cancer Manag. Res.* **2019**, *11*, 4971–4984. [[CrossRef](#)]
15. Piat, A.P.; Tirosh, I.; Trombetta, J.J.; Shalek, A.K.; Gillespie, S.M.; Wakimoto, H.; Cahill, D.P.; Nahed, B.V.; Curry, W.T.; Martuza, R.L.; et al. Single-Cell RNA-Seq Highlights Intratumoral Heterogeneity in Primary Glioblastoma. *Science* **2014**, *344*, 1396–1401. [[CrossRef](#)]
16. Sottoriva, A.; Spiteri, I.; Piccirillo, S.G.M.; Touloumis, A.; Collins, V.P.; Marioni, J.C.; Curtis, C.; Watts, C.; Tavaré, S. Intratumor Heterogeneity in Human Glioblastoma Reflects Cancer Evolutionary Dynamics. *Proc. Natl. Acad. Sci. USA* **2013**, *110*, 4009–4014. [[CrossRef](#)]
17. Kuo, M.D.; Jamshidi, N. Behind the Numbers: Decoding Molecular Phenotypes with Radiogenomics—Guiding Principles and Technical Considerations. *Radiology* **2014**, *270*, 320–325. [[CrossRef](#)]
18. Mazurowski, M.A. Radiogenomics: What It Is and Why It Is Important. *J. Am. Coll. Radiol.* **2015**, *12*, 862–866. [[CrossRef](#)]
19. Gillies, R.J.; Kinahan, P.E.; Hricak, H. Radiomics: Images Are More than Pictures, They Are Data. *Radiology* **2016**, *278*, 563–577. [[CrossRef](#)]
20. Van Timmeren, J.E.; Cester, D.; Tanadini-Lang, S.; Alkadhi, H.; Baessler, B. Radiomics in Medical Imaging—“How-to” Guide and Critical Reflection. *Insights. Imaging.* **2020**, *11*, 91. [[CrossRef](#)]
21. Jian, A.; Jang, K.; Manuguerra, M.; Liu, S.; Magnussen, J.; Di Ieva, A. Machine Learning for the Prediction of Molecular Markers in Glioma on Magnetic Resonance Imaging: A Systematic Review and Meta-Analysis. *Neurosurgery* **2021**, *89*, 31–44. [[CrossRef](#)] [[PubMed](#)]
22. LeCun, Y.; Bengio, Y.; Hinton, G. Deep Learning. *Nature* **2015**, *521*, 436–444. [[CrossRef](#)] [[PubMed](#)]
23. Charron, O.; Lallement, A.; Jarnet, D.; Noblet, V.; Clavier, J.-B.; Meyer, P. Automatic Detection and Segmentation of Brain Metastases on Multimodal MR Images with a Deep Convolutional Neural Network. *Comput. Biol. Med.* **2018**, *95*, 43–54. [[CrossRef](#)] [[PubMed](#)]
24. Rudie, J.D.; Weiss, D.A.; Saluja, R.; Rauschecker, A.M.; Wang, J.; Sugrue, L.; Bakas, S.; Colby, J.B. Multi-Disease Segmentation of Gliomas and White Matter Hyperintensities in the BraTS Data Using a 3D Convolutional Neural Network. *Front Comput. Neurosci.* **2019**, *13*, 84. [[CrossRef](#)] [[PubMed](#)]
25. Buda, M.; AlBadawy, E.A.; Saha, A.; Mazurowski, M.A. Deep Radiogenomics of Lower-Grade Gliomas: Convolutional Neural Networks Predict Tumor Genomic Subtypes Using MR Images. *Radiol. Artif. Intell.* **2020**, *2*, e180050. [[CrossRef](#)]
26. Cluceru, J.; Interian, Y.; Phillips, J.J.; Molinaro, A.M.; Luks, T.L.; Alcaide-Leon, P.; Olson, M.P.; Nair, D.; LaFontaine, M.; Shai, A.; et al. Improving the Noninvasive Classification of Glioma Genetic Subtype with Deep Learning and Diffusion-Weighted Imaging. *Neuro. Oncol.* **2021**, *24*, noab238. [[CrossRef](#)]
27. Fu, J.; Singhrao, K.; Zhong, X.; Gao, Y.; Qi, S.X.; Yang, Y.; Ruan, D.; Lewis, J.H. An Automatic Deep Learning-Based Workflow for Glioblastoma Survival Prediction Using Preoperative Multimodal MR Images: A Feasibility Study. *Adv. Radiat. Oncol.* **2021**, *6*, 100746. [[CrossRef](#)]
28. Han, W.; Qin, L.; Bay, C.; Chen, X.; Yu, K.-H.; Miskin, N.; Li, A.; Xu, X.; Young, G. Deep Transfer Learning and Radiomics Feature Prediction of Survival of Patients with High-Grade Gliomas. *AJNR Am. J. Neuroradiol.* **2020**, *41*, 40–48. [[CrossRef](#)]
29. Pedano, N.; Flanders, A.E.; Scarpace, L.; Mikkelsen, T.; Eschbacher, J.M.; Hermes, B.; Sisneros, V.; Barnholtz-Sloan, J.; Ostrom, Q. The Cancer Genome Atlas Low Grade Glioma Collection (TCGA-LGG) (Version 3) [Data set]. *Cancer Imaging Archive* **2016**. [[CrossRef](#)]
30. Clark, K.; Vendt, B.; Smith, K.; Freymann, J.; Kirby, J.; Koppel, P.; Moore, S.; Phillips, S.; Maffitt, D.; Pringle, M.; et al. The Cancer Imaging Archive (TCIA): Maintaining and Operating a Public Information Repository. *J. Digit. Imaging.* **2013**, *26*, 1045–1057. [[CrossRef](#)]
31. Li, X.; Morgan, P.S.; Ashburner, J.; Smith, J.; Rorden, C. The First Step for Neuroimaging Data Analysis: DICOM to NIFTI Conversion. *J. Neurosci. Methods* **2016**, *264*, 47–56. [[CrossRef](#)]
32. Tustison, N.J.; Avants, B.B.; Cook, P.A.; Zheng, Y.; Egan, A.; Yushkevich, P.A.; Gee, J.C. N4ITK: Improved N3 Bias Correction. *IEEE Trans. Med. Imaging.* **2010**, *29*, 1310–1320. [[CrossRef](#)]
33. Smith, S.M. Fast Robust Automated Brain Extraction. *Hum. Brain Mapp.* **2002**, *17*, 143–155. [[CrossRef](#)]

34. Jenkinson, M.; Bannister, P.; Brady, M.; Smith, S. Improved Optimization for the Robust and Accurate Linear Registration and Motion Correction of Brain Images. *NeuroImage* **2002**, *17*, 825–841. [[CrossRef](#)]
35. Shinohara, R.T.; Sweeney, E.M.; Goldsmith, J.; Shiee, N.; Mateen, F.J.; Calabresi, P.A.; Jarso, S.; Pham, D.L.; Reich, D.S.; Crainiceanu, C.M. Statistical Normalization Techniques for Magnetic Resonance Imaging. *NeuroImage Clinical*. **2014**, *6*, 9–19. [[CrossRef](#)]
36. Zhou, H.; Vallières, M.; Bai, H.X.; Su, C.; Tang, H.; Oldridge, D.; Zhang, Z.; Xiao, B.; Liao, W.; Tao, Y.; et al. MRI Features Predict Survival and Molecular Markers in Diffuse Lower-Grade Gliomas. *Neuro. Oncol.* **2017**, *19*, 862–870. [[CrossRef](#)] [[PubMed](#)]
37. Ioffe, S.; Szegedy, C. Batch Normalization: Accelerating Deep Network Training by Reducing Internal Covariate Shift. *arXiv* **2015**, arXiv:1502.03167.
38. Lin, M.; Chen, Q.; Yan, S. Network In Network. *arXiv* **2013**, arXiv:1312.4400. [[CrossRef](#)]
39. Kingma, D.P.; Ba, J. Adam: A Method for Stochastic Optimization. *arXiv* **2014**, arXiv:1412.6980. [[CrossRef](#)]
40. R Core Team. *R: A Language and Environment for Statistical Computing*; R Foundation for Statistical Computing: Vienna, Austria, 2018.
41. RStudio Team RStudio. *Integrated Development for R*. RStudio, PBC, Boston, MA; PBC: Boston, MA, USA, 2020.
42. Zhang, Q.; Liu, W.; Luo, S.-B.; Xie, F.-C.; Liu, X.-J.; Xu, R.-A.; Chen, L.; Su, Z. Development of a Prognostic Five-Gene Signature for Diffuse Lower-Grade Glioma Patients. *Front. Neurol.* **2021**, *12*, 633390. [[CrossRef](#)]
43. Liu, W.; Zou, J.; Ren, R.; Liu, J.; Zhang, G.; Wang, M. A Novel 10-Gene Signature Predicts Poor Prognosis in Low Grade Glioma. *Technol. Cancer Res. Treat.* **2021**, *20*, 153303382199208. [[CrossRef](#)] [[PubMed](#)]
44. Zhang, M.; Wang, X.; Chen, X.; Zhang, Q.; Hong, J. Novel Immune-Related Gene Signature for Risk Stratification and Prognosis of Survival in Lower-Grade Glioma. *Front. Genet.* **2020**, *11*, 363. [[CrossRef](#)]
45. Manikis, G.C.; Ioannidis, G.S.; Siakallis, L.; Nikiforaki, K.; Iv, M.; Vozlic, D.; Surlan-Popovic, K.; Wintermark, M.; Bisdas, S.; Marias, K. Multicenter DSC–MRI-Based Radiomics Predict IDH Mutation in Gliomas. *Cancers* **2021**, *13*, 3965. [[CrossRef](#)] [[PubMed](#)]
46. Kickingeder, P.; Sahm, F.; Radbruch, A.; Wick, W.; Heiland, S.; von Deimling, A.; Bendszus, M.; Wiestler, B. IDH Mutation Status Is Associated with a Distinct Hypoxia/Angiogenesis Transcriptome Signature Which Is Non-Invasively Predictable with RCBV Imaging in Human Glioma. *Sci. Rep.* **2015**, *5*, 16238. [[CrossRef](#)] [[PubMed](#)]

Disclaimer/Publisher’s Note: The statements, opinions and data contained in all publications are solely those of the individual author(s) and contributor(s) and not of MDPI and/or the editor(s). MDPI and/or the editor(s) disclaim responsibility for any injury to people or property resulting from any ideas, methods, instructions or products referred to in the content.